TOPICAL REVIEW — 2D materials: physics and device applications

Photodetectors based on junctions of two-dimensional transition metal dichalcogenides*

Xia Wei(魏侠)[1], Fa-Guang Yan(闫法光)[1], Chao Shen(申超)[1], Quan-Shan Lv(吕全山)[1], and Kai-You Wang(王开友)[1,2,†]

[1] State Key Laboratory of Superlattices and Microstructures, Institute of Semiconductors, Chinese Academy of Sciences, Beijing 100083, China
[2] College of Materials Science and Opto-Electronic Technology, University of Chinese Academy of Science, Beijing 100049, China

(Received 20 December 2016; revised manuscript received 21 January 2017; published online 13 February 2017)

Transition metal dichalcogenides (TMDCs) have gained considerable attention because of their novel properties and great potential applications. The flakes of TMDCs not only have great light absorption from visible to near infrared, but also can be stacked together regardless of lattice mismatch like other two-dimensional (2D) materials. Along with the studies on intrinsic properties of TMDCs, the junctions based on TMDCs become more and more important in applications of photodetection. The junctions have shown many exciting possibilities to fully combine the advantages of TMDCs, other 2D materials, conventional and organic semiconductors together. Early studies have greatly enriched the application of TMDCs in photodetection. In this review, we investigate the efforts in photodetectors based on the junctions of TMDCs and analyze the properties of those photodetectors. Homojunctions based on TMDCs can be made by surface chemical doping, elemental doping and electrostatic gating. Heterojunction formed between TMDCs/2D materials, TMDCs/conventional semiconductors and TMDCs/organic semiconductor also deserve more attentions. We also compare the advantages and disadvantages of different junctions, and then give the prospects for the development of junctions based on TMDCs.

Keywords: transition metal dichalcogenides, homojunction, heterojunction, photodetector

PACS: 85.30.Kk, 85.60.Bt, 85.60.Dw **DOI:** 10.1088/1674-1056/26/3/038504

1. Introduction

Since the discovery of graphene by Geim and Novoselov,[1,2] many unique properties[3–7] have emerged, resulting in considerable attention on layered materials.[8–11] Many efforts have been put into the fundamental physical researches on properties of layered materials for next generation of electronics and optoelectronics. Until now there have already been hundreds of layered materials that can be thinned down to monolayers and retain their stability.[3] Each layered material has its own merits and demerits. For example, the carrier mobility in black phosphorus (BP) is higher than that in transition metal dichalcogenides (TMDCs), but TMDCs have larger light absorption compared with BP in visible range.

TMDCs have the general formula MX_2 where M is a transition metal (such as Mo, W) and X is a chalcogen atom (such as S, Se, Te).[12–15] The atoms forming bounds are arranged into planes (layers). The layers are combined by van der Waals interactions to form bulk crystals.[16] The weak out-of-plane interactions allow the isolation of single layers by micromechanical exfoliation.

Crystals of TMDCs have been investigated for more than five decades.[16,17] However, only in past decade, the thin layers of TMDCs were set off an upsurge, where many interesting properties were observed, such as charge density wave, superconductivity, variation of band structure, and so on.[12,18,19] Among them, the variation of band structure is prominent in optical properties. For example, the bandgaps of TMDCs change from indirect to direct when the TMDCs are thinned down to monolayers. The direct bandgap leads to increased probability for photon to generate electron-hole pairs which results in better light absorptions. Moreover the bandgaps of thin layered TMDCs rely on the number of layers,[12,13,20–24] which allows the absorption of light at different wavelength. Due to the van der Waals interactions between layers, we can also stack different types of TMDC flakes regardless of lattice mismatching to have different wavelength light absorption.[25]

Earlier, photodetectors based on field-effect transistor (FET) structure of TMDCs have been studied[26–31] and have shown excellent performances, such as the highest photoresponsivity of 880 $A{\cdot}W^{-1}$ based on monolayer MoS_2.[31] There have already been many reviews.[24,25,32–36] Because the built-in electric field can effectively separate photogenerated electron–hole pairs, the junctions of TMDCs have gained more attentions for optoelectronics in these years. With the rapid development of the photodetectors based on the junctions of TMDCs, it is time to review the recent achievements. In this review, we mainly present photodetectors based on junctions of TMDCs flakes utilizing photoconductive effect and photo-

*Project supported by the National Basic Research Program of China (Grant No. 2014CB643903), the National Natural Science Foundation of China (Grant Nos. 61225021, 11474272, 11174272, and 11404324), and K. C. Wong Education Foundation.

†Corresponding author. E-mail: kywang@semi.ac.cn

© 2017 Chinese Physical Society and IOP Publishing Ltd

voltaic effect. Firstly the underlying physics of photodetection based on P-N junctions are briefly introduced. We then will discuss and compare the different kinds of junctions based on TMDCs (including techniques and performances). After that, we conclude the advantages and disadvantages of different junctions. Finally we give the prospects for the future developments of junctions based on TMDCs.

2. Two main mechanisms of photodetection: photoconductive effect and photovoltaic effect

Different materials normally have different work functions and Fermi levels. When junctions are formed between p type and n type materials, the band structures will change due to the alignment of the Fermi levels. The conduction and valance band edge of p type materials will bend down. On the contrary, the conduction and valance band edge of n type materials will bend up. Then the energy barrier will be generated between the two materials.

In the photoconductive effect, when the photon energy is higher than the bandgap, photon absorptions generate extra electron–hole pairs. The photogenerated electrons and holes can be drifted in opposite directions by built-in electric field and external source-drain voltage, which greatly reduces recombination of electron–hole pairs and generates photocurrent (Fig. 1(a)). The photocurrent adds to the dark current, resulting in the reduction of the resistance. Under negative external voltage, the internal electric field will be enhanced and the energy barrier will increase by qV_R (Fig. 1(a)). Photogenerated electrons are easier to be drifted to low energy side (the side of n type material) and photogenerated holes are easier to be drifted to low energy side (the side of p type material). Thus, the photogenerated electrons and holes are separated more effectively.

In the photovoltaic effect, photocarriers are also generated in the same way as the photoconductive effect. However, the difference lies in that photogenerated electron–hole pairs are separated only by built-in electric filed rather than external field V_{ds}. The built-in electric field generally exists in PN junctions or Schottky junctions. The built-in electric field can effectively separate electrons and holes, which leads to a sizeable short-current I_{sc} at $V_{ds} = 0$. Moreover, when the circuit is open, photocarriers will be accumulated on both sides, and open circuit voltage V_{oc} can be obtained (Fig. 1(b)).

There are two operating modes for the PN junction photodetectors: photoconductive mode (the photodetectors work under external bias, Fig. 1(a)) and photovoltaic mode (the photodetectors work without external electric field, Fig. 1(b)). The advantage of photovoltaic mode is the lowest dark current which improves the specific detectivity. The advantages of the photoconductive mode are as follows: i) the reduction of the junction capacitance increases the response speed; ii) under reverse bias, the recombination probability of the photogenerated electrons and holes are smaller, making it suitable for weak light detection; iii) under reverse bias, the width of depletion layer will be extended, which will increasing photon collection efficiency.

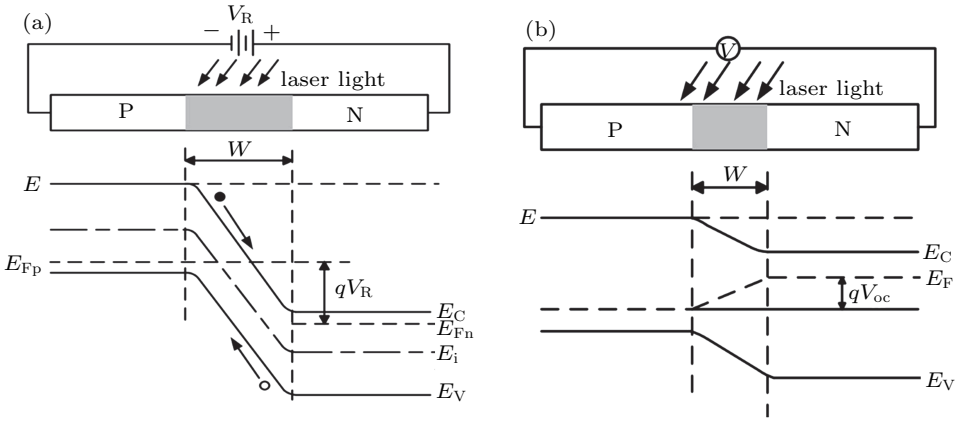


Fig. 1. (a) Band alignment of PN junction under photoconductive mode. (b) Band alignment of PN junction under photovoltaic mode.

To facilitate comparison of the photodetectors, we mainly focus on the following figures of merits of photodetectors based on junctions: external quantum efficiency (EQE), responsivity (R), specific detectivity (D^*), and response time (τ).

External quantum efficiency is a ratio between the number of the charge carriers generated and the number of incident photons on photodetectors. It depends on both the absorption of light and collection of the charges. Responsivity is the ratio between the photocurrent and the incident light power density on photodetectors, which implies the achievable electrical signal under certain illumination. Specific detectivity is equal to the reciprocal of noise-equivalent power, normalized per square root of the sensor's area and frequency bandwidth, which indicates the measure of detector sensitivity. The time response of detectors is measured between 10% and 90% of the final output signal, either on the rising or falling edge.

3. Photodetectors based on homojunctions of TMDCs

In conventional semiconductors, homojunctions are the semiconductor interfaces that occur at the similar semiconductor materials with equal bandgaps and different doping. Similarly, homojunctions exist at the interface of 2D materials such as graphene,[37–39] WSe_2,[40–43] and black phosphorus.[44] In conventional semiconductors, elemental doping is the most common way to form the homojunctions. However, there are three ways to modulate the carrier type of TMDCs to create homojunctions. The first one is to change the surface properties via chemical treatment.[45–48] The second one is to change the properties of the single-crystalline TMDCs by elemental doping.[49,50] The homojunctions can also be created by electrostatic gating except for doping.[40–43] In the following, we will review the recent development concerning the homojunctions created by these three methods respectively.

3.1. Homojunction fabricated by surface chemical doping

In 2012, Hui *et al.* obtained p-doped WSe_2 using physisorbed NO_2. However, the doping decays almost within an hour because of the weak physisorption process.[51] Next year they realized n-doping of WSe_2 and MoS_2 by Pstassium, which could decrease the contact resistance.[45] Surface chemical doping is demonstrated to lead to the conduction transition of thin TMDC layers. Lately, lateral homojunction devices based on surface chemical doping were presented by Choi *et al.* in Fig. 2(a).[46] The stacks of MoS_2 and boron nitride (BN) flakes in the devices rely on the mechanical exfoliation and transfer. BN was partially covered on MoS_2 by polydimethysiloxane stamp. The $AuCl_3$ chemical dopant was spin-coated onto the partially stacked h-BN/MoS_2 heterostructure.

The Au nanoaggregates can form due to the reduction of $AuCl_4^{-1}$ ions in the $AuCl_3$ solution. Because of the reaction, the ions which are in direct contact with MoS_2 can receive electrons from MoS_2 layers. Thus, the p-type MoS_2 will be formed by surface charge transfer, and then the homojunctions of P–N junctions based on MoS_2.

The log-plotted I_{ds}–V_{ds} curves under different gate configurations show the reverse current can be decreased with increasing V_g, which is very useful for photodetectors. The large tunable conductance can be attributed to the gating tuning Fermi surface towards or backwards the valance band, which changes the hole transport. Meanwhile, the curves in Fig. 2(b) imply the rectifications resulting from the chemical doping.

Figure 2(c) plots the EQE (left axis) and D^* (right axis) for different wavelength of light. The maximum EQE obtained is $\sim 7000\%$ at $V_{ds} = 1.5$ V, $V_g = -40$ V, and 350 nm. It is worth noting that the EQE under different conditions is around 100 times higher than that of the intrinsic MoS_2 phototransistor.[53] Meanwhile the obtained D^* is similar to the reported multilayer intrinsic MoS_2 phototransistors. Therefore the $AuCl_3$ doping and stacking processes have not influenced the sensitivity of the devices.

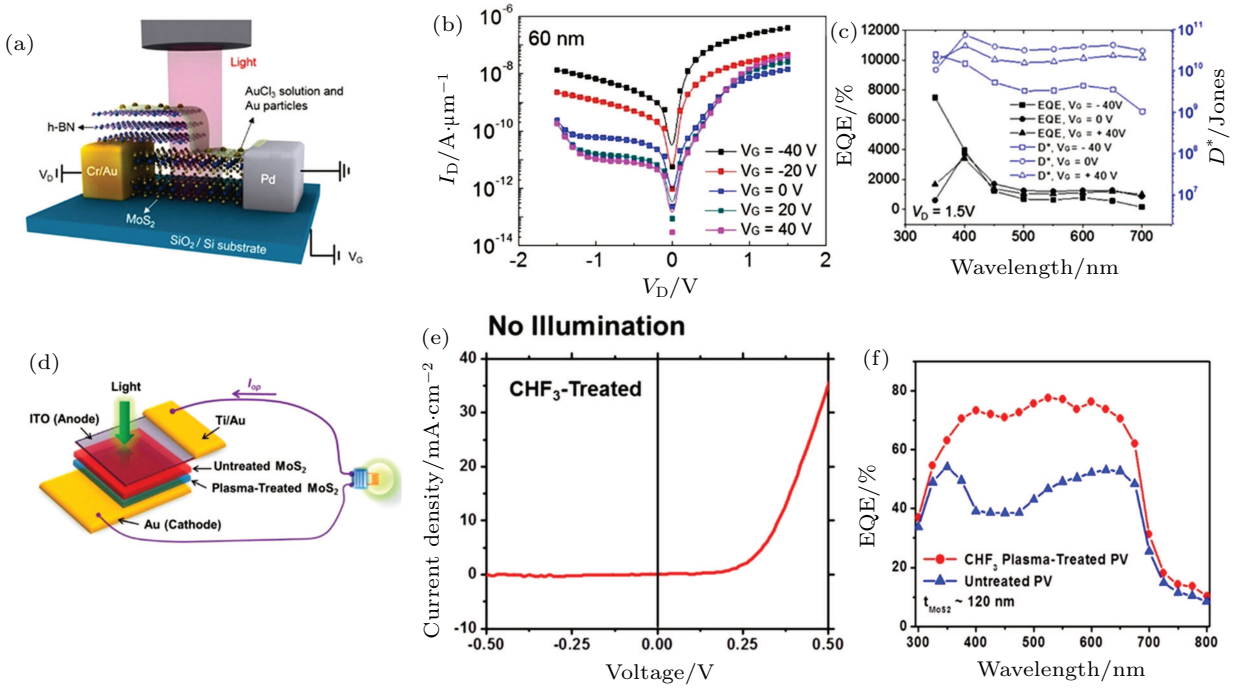


Fig. 2. (color online) (a) Lateral device schematic diagram of PN junction by $AuCl_3$ chemical dopant.[46] (b) I_{ds}–V_{ds} characteristics measured in different gate configurations.[46] (c) EQE and D^* with respect to the wavelength of light at $V_{ds} = +1.5$ V and $V_g = 0$, 40 V and -40 V.[46] (d) Vertical PN junction schematic with CHF_3 plasma-treated MoS_2 layers.[52] (e) J_{ds}–V_{ds} characteristics of CHF_3 plasma-treated PN junctions.[52] (f) EQE under different wavelength of light.[52]

Another example presented here is the MoS_2 P–N junctions fabricated by CHF_3 plasma doping.[52] As shown in Fig. 2(e), the junction exhibits more prominent diode-like behavior than the Au/untreated MoS_2/ITO heterostructure. The junction formed at CHF_3 treated and untreated MoS_2 surfaces shows the built-in potential of 0.7 eV. Under photovoltaic mode, the EQE of CHF_3 treated MoS_2 PN junction can reach a high value of 78%.

In 2016, Lei *et al.* fabricated planer p–n junctions based on 2D InSe by making use of the long pair electrons found in most of 2D metal chalcogenides rather than relying on lattice defects and physisorption methods.[48] Via a Lewis acid-base reaction, the long pair electrons of n type InSe can react with Ti^{4+} to form p type coordination complexes. Moreover the conduction type conversion in other 2D materials can also be realized via Lewis acids.

To conclude, surface chemical doping is an effective way to prepare photodetectors based on the homojunctions of TMDCs without influencing the sensitivity of the photodetectors. Not only under photoconductive mode but also under photovoltaic mode, the homojunctions have shown higher EQE than the intrinsic TMDCs. Moreover chemical surface doping can also be used to decrease the contact resistance between TMDCs and metal. However, the properties of the homojunctions of TMDCs made by surface chemical doping can easily be affected by external environment. Thus the stability of these devices is rather poor.

3.2. Homojunctions fabricated by elemental doping

To have more stable and controllable PN junction, elemental doping has been used to create the homojunctions. Practical applications require substitution of host atoms with dopants, where the doping is secured and stabilized by covalent bonding inside the lattice. Suh *et al.*[49] realized stable P-type doping in bulk MoS_2 by substitutional niobium (Nb) and achieved degenerate hole density of $\sim 3 \times 10^{19}$ cm^{-3}. In order to form p-type $MoSe_2$, Jin *et al.* also used Nb with five valance electrons to replace Mo which has six valance electrons.[50] Via Nb doping, n-type $MoSe_2$ single crystal can be successfully converted to p-type (Fig. 3(a)). The thin n-$MoSe_2$ and p-$MoSe_2$ layers were stacked by mechanical exfoliation and transfer. Then the vertical homojunctions based on layered $MoSe_2$ have been realized on SiO_2/Si substrates (see insets in Fig. 3(b)).

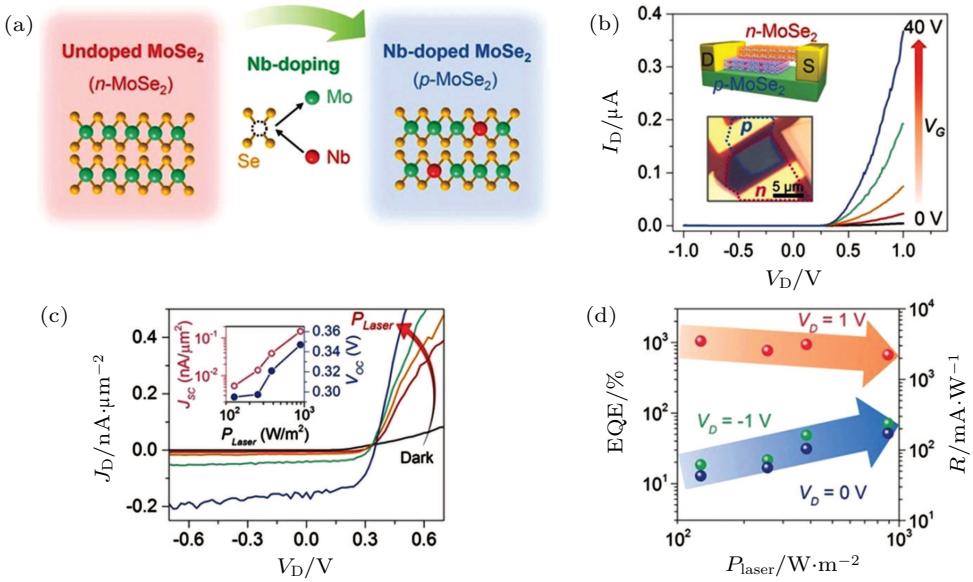


Fig. 3. (color online) (a) Schematic diagram of Nb-doping for converting n-$MoSe_2$ to p-$MoSe_2$. (b) I_{ds}–V_{ds} characteristics measured in different gate configurations. The insets: optical image and schematic of the vertical homojunctions based on $MoSe_2$. (c) J_d–V_{ds} curves under different laser powers. The inset: short circuit current and open circuit voltage as a function of P_{Laser}. (d) EQE and D^* with respect to the laser power under different V_{ds}.[50]

The fabricated p–n junction exhibits typical rectification properties, as shown in Fig. 3(b). Not only that, the ideality factor was calculated to be $\sim$1, which implies the device is an ideal diode. With increasing illuminated light intensity, short-circuit current (I_{sc}), open-circuit voltage (V_{oc}) and reverse current are all increased, as shown in Fig. 3(c). This is consistent with the photovoltaic mechanism where the generated photocurrent can add to the reverse current. In Fig. 3(d), both the EQE and the responsivity are enhanced at $V_{ds} = 0$ and $V_{ds} = -1$ V as the laser power increased. Photocarriers can be more easily drifted to electrode across the depletion region under reverse bias. For the vertical $MoSe_2$ homojunction by elemental doping, the maximum EQE and R value can reach $\sim$ 1049% and be more than 1 A·W^{-1} at $V_{ds} = 1$ V, $P_{Laser} = 890$ W·m^{-2}, respectively.

The elemental doping is superior in terms of versatility

and stability over surface chemical treatment based on absorption or intercalation of volatile species. However, the elemental doping is more suitable for TMDC bulk materials rather than very few layered materials. In order to fabricate PN junctions based on the few-layer TMDCs, mechanical exfoliation is often essential, which can induce uncertainty factors such as the thicknesses and the resistance between the flakes. Thus, the current method is not suitable for practical application. Recently, Kim *et al*. realized phosphorus doping in monolayer and bilayer MoS_2 by laser.[54] This approach can be controlled effectively by varying the laser irradiation power and time. However, more solutions of elemental doping in thin layers are still needed. We expect to realize PN homojunctions based on layered TMDCs through the elemental doping during the CVD growth, which is important for the application of TMDCs.

3.3. Homojunction fabricated by electrostatic gating

Unlike other TMDCs such as MoS_2, $MoSe_2$, and WS_2, WSe_2 has been demonstrated to be ambipolar transport.[40–42,55] The carrier type of WSe_2 can be controlled through electrostatic gating. The homojunction based on WSe_2 has been created successfully by this method.[40]

The schematic diagram of the locally-gated junction is presented in Fig. 4(a). The single-layer WSe_2 flake was transferred on two local gates covered with BN as a dielectric layer. Except BN,[40,42,56] conventional dielectrics such as HfO_2,[41] Si_3N_4,[43] Al_2O_3[39] have also been used in similar type devices. Compared with HfO_2 and Si_3N_4, BN flake has atomically flat surface and charge traps-free interface, it can improve the interface between BN and WSe_2, thus enhance the mobility of devices.

In Fig. 4(b), the ambipolar I_{ds} can be controlled by V_g, implying both hole and electron-doping can be accessed. This phenomenon can be attributed to that the Femi level E_F can be effectively moved up and down across the bandgap by V_g in thin layers of WSe_2. The moving of E_F to the conductive band or valance band will induce different carrier types and concentrations. Similar behavior has also been reported by others.[42,43] So the types of the junctions (PP, PN and NN) can be adjusted by controlling V_{lg} and V_{rg}, as shown in Fig. 4(c).

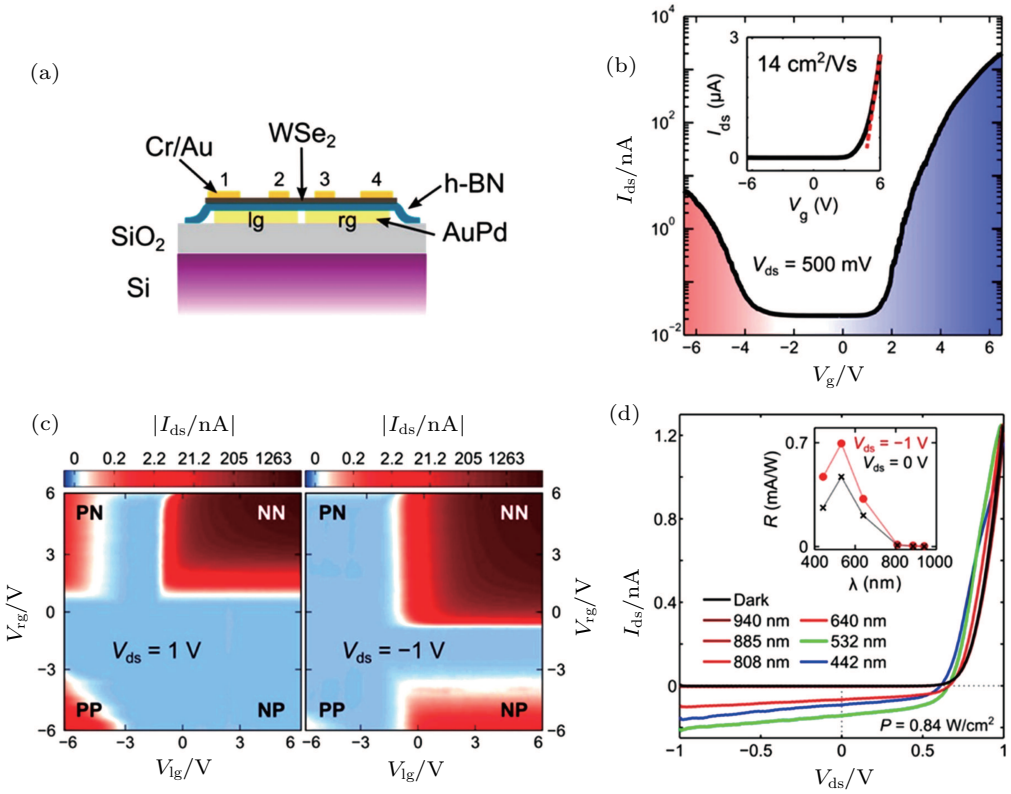


Fig. 4. (color online) (a) Device schematic diagram. (b) The log plotted I_{ds}–V_g curve was measured under $V_{ds} = 500$ mV. The color gradient implies the transition between hole- and electron-doping. Inset shows the data on a linear scale. (c) Color maps of I_{ds} under different V_{lg}, V_{rg} and V_{ds} which suggest the types of the junctions. (d) I_{ds}–V_{ds}characteristics under different illumination wavelength. The inset shows the responsivity (R) under $V_{ds} = -1$ V and $V_{ds} = 0$.[40]

Then we focus on the photoresponse of the PN junction formed by electrical gating. The maximum responsivity is 0.7 mA·W^{-1} at $V_{ds} = -1$ V and 532 nm illuminations. Meanwhile the EQE reaches a maximum value of 0.1%. In addition, the response time is in the order of 10 ms. Though the EQE here is lower compared with the two doping methods mentioned above, locally electrostatic gating is still a novel way to tune the junctions and control their electrical properties.

To conclude, the homojunction photodetectors based on TMDCs have been introduced, which can be realized by three

different ways: surface chemical doping, elemental doping and electrostatic gating. Compared with intrinsic TMDCs, photodetectors based on homojunctions can largely improve the EQE and *R*. Meanwhile homojunctions are fabricated by only one kind of TMDCs, which makes them promising as detectors for special wavelength applications from visible to near infrared.

4. Photodetectors based on heterojunctions of TMDCs

In contrast to homojunctions, heterojunction is the semiconductor interface that occurs between two dissimilar materials with unequal bandgaps. Flakes of TMDCs can be placed on conventional semiconductor materials, organic semiconductor or on other 2D materials by ways such as CVD, mechanical exfoliation and transfer and so on. Due to the unique layer thickness dependence of the bandgaps, the heterojunctions can also be made of only single TMDCs with two different layer thickness.

4.1. Heterojunctions based on TMDCs, conventional bulk semiconductors, and organic semiconductors

4.1.1. Heterojunctions based on TMDCs and conventional bulk semiconductors

Compared with heterojunctions based on two different 2D materials, it is easier and more feasible to combine a 2D layered material with conventional semiconductor materials such as MoS_2/Si,[57–62] WSe_2/InAs,[63] MoS_2/GaAs,[64] and MoS_2/GaN.[65]

The MoS_2/Si heterojunctions have been widely investigated.[57–62] Most of such junctions were fabricated by mechanical exfoliation and transfer.[57–60] Esmaeili-Rad *et al*. fabricated heterojunction of MoS_2/a-Si and they obtained the photoresponsivity of 210 mA/W at green light.[57] Vertical MoS_2/p-Si heterojunction was fabricated by transferring and the high photoresponsivity of 7.2 A/W was obtained.[60] In order to have large scale such heterojunctions, Wang *et al*.[61] and Hao *et al*.[62] fabricated the MoS_2/Si heterojunctions by magnetron sputtering.

Figure 5(a) shows the device geometry fabricated by Wang *et al*.[61] The MoS_2 film was deposited on the p-Si substrate with a predefined SiO_2 window by magnetron sputtering. The deposited molecular layers of MoS_2[61] are perpendicular to the substrate as shown in Fig. 5(b), which is different from the MoS_2 prepared by mechanical exfoliation[57,59,60] and chemical vapour deposition.[58]

The I_{sc} and V_{oc} increase with the increased light intensity in Fig. 5(c), which strongly suggests that photocarriers are separated by the electric field at the interface of MoS_2 and Si. Responsivity can reach ~ 300 mA·W^{-1} under the light intensity of 1 mW·cm^{-2} which is comparable to most of the devices based on MoS_2.[26,50,57,66] The maximum value of specific detectivity is $\sim 10^{13}$ Jones at 1 mW·cm^{-2} which is three orders of magnitude higher than MoS_2/Si heterojunction photodetectors by transferring.[60]

The rising and decaying time of the MoS_2/Si heterojunctions were calculated to be 3 μs and 40 μs, which is by far the reported fastest response in TMDCs heterojunctions. The fast response is directly related with the structure and can be attributed to the following reasons: the strong build-in electric field which can efficiently separate photocarriers; the vertically standing layered structure of MoS_2 layers which offers high-speed paths; thin SiO_2 between Si and MoS_2 which serves as a passivation layer to reduce the interface defects.

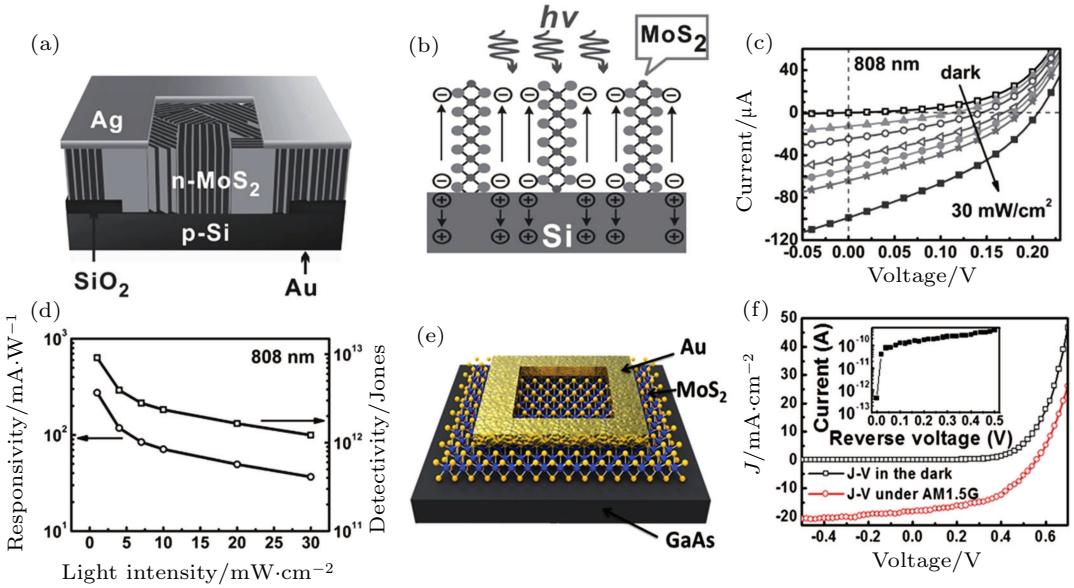


Fig. 5. (color online) (a) Device schematic of the MoS_2/Si heterojunction photodetector.[61] (b) Schematic illustration shows the separation of the photocarriers under illumination.[61] (c) Photoresponse characteristics measured under different light intensities of 808 nm laser.[59] (d) Responsibility and specific detectivity with respect to the light intensity.[61] (e) Schematic structure of MoS_2/GaAs heterojunction.[64] (f) Current density-voltage curves of MoS_2/GaAs heterojunction under dark and illumination.[64]

Lately, Xu *et al.* developed MoS_2/GaAs heterojunctions which have wide response band width from ultraviolet to visible light.[64] In order to decrease the dark current, h-BN was inserted into the interface between MoS_2 and GaAs. Owing to h-BN, the detectivity can reach 1.9×10^{14} Jones which is even higher than that of MoS_2/Si heterojunction.[61] MoS_2/GaN heterojunctions have also been prepared by Ruzmetov *et al.* via power vaporization technique and show very high-quality van der Waals interface.[65]

The MoS_2/Si heterojunctions show not only high specific detectivity but also short response time.[61] The photodetectors based on MoS_2/GaAs heterojunctions have wider photoresponse band width. The efforts above confirm that combining 2D TMDCs with conventional semiconductor technology is a promising way to make high performances PN heterostructural photodetectors.

4.1.2. Heterojunctions based on TMDCs and organic semiconductor

Compared with conventional bulk semiconductor, much cheaper organic semiconductor materials including pentacene,[67,68] C_8-BTBT,[69–71] CuPc,[72] and PTCDA[73] have also enriched the design of heterojunction based on TMDCs.

A lot of efforts have been made to epitaxially grow organic semiconductor thin film on 2D materials such as graphene, BN, and MoS_2. He *et al.* grew high-quality few layer C_8-BTBT on graphene and BN via van der Waals epitaxy. The thickness of C_8-BTBT can be well controlled down to monolayer.

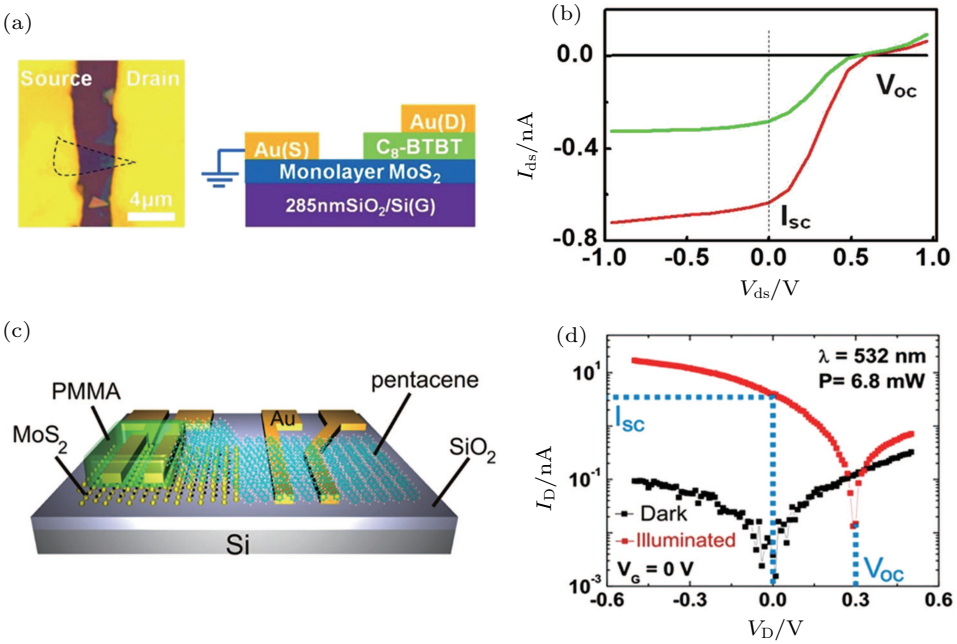


Fig. 6. (color online) (a) Microscope image and device schematic of vertical C_8-BTBT/ MoS_2 heterojunction.[70] (b) I_{ds}–V_{ds} under white light illumination with different power.[70] (c) Structure of pentacene/ MoS_2 heterojunction.[67] (d) I_{ds}–V_{ds} under dark and illumination.[67]

Lately the heterojunctions based on monolayer MoS_2 and p-type C_8-BTBT in Fig. 6(a) were also presented by He *et al.*[70] MoS_2 was mechanically exfoliated on SiO_2/Si as an epitaxy substrate and then few-layer C_8-BTBT on MoS_2 was grown by epitaxial growth. The sharp and clean interface can be formed between the MoS_2 and the organic C_8-BTBT, which is important for the performance of the heterojunction. Under illumination, obvious I_{sc} and V_{oc} response are observed in the heterojunction as shown in Fig. 6(b) and the responsibility can reach 22 mA/W under photovoltaic mode. At the same time, Jariwala *et al.* fabricated heterojunctions based on MoS_2 and p-type pentacene.[67] As shown in Fig. 6(d), the devices show apparent diode-like behavior and large photoresponse. This kind of hybrid heterojunctions has attracted a lot of attention and can show good performances by selecting appropriate device structures and materials. Compared with conventional semiconductors, organic semiconductors can be made in inexpensive methods. Moreover the low annealing temperature of organics allows for flexibility of substrate choice. It is promising to fabricate cheaper photodetectors by combining TMDCs and organic semiconductors.

4.2. Photodetectors based on heterojunctions of only TMDCs

4.2.1. Fabrication of heterojunctions based on only TMDCs

Because of the weak van der Waals interactions, we can stack any two kinds of 2D materials together in order to form heterojunctions by mechanical exfoliation and transfer regardless of the lattice mismatch, which will give us

wide variety selections of layered materials. A lot of efforts have been made to stack vertical heterojunctions of 2D TMDCs by mechanical exfoliation and transfer as shown in heterojunctions such as MoS_2/WS_2,[74,75] MoS_2/WSe_2,[76–82] $MoS_2/MoSe_2$,[83] $MoS_2/MoTe_2$,[84] $MoSe_2/WSe_2$,[85] and so on. Although such vertical heterojunctions show very good performance in photodetection, the yield and efficiency of making such devices is very low.

In order to reduce the steps of mechanical exfoliation and transfer, Cheng *et al.* combine physical vapor deposition process, mechanical exfoliation, and transfer together.[86] However, the efficiency and the quality of junctions still have not been improved much.

Since MoS_2 layers were grown by chemical vapor deposition (CVD),[87–89] CVD has been regarded as a feasible and efficient way to directly fabricate heterojunctions on a large scale. Moreover, CVD-grown devices showed stronger interlayer interaction compared with their transferred counterparts.

In 2014, Gong *et al.*[90] grew both vertical and lateral MoS_2/WS_2 heterojunctions by CVD. As the FET, the vertical MoS_2/WS_2 heterojunctions have very high ON/OFF ratio of 10^6 and the estimated mobility is in the range of 15 to 34 $cm^2 \cdot V^{-1} \cdot s^{-1}$, which is faster than MoS_2/WS_2 made by mechanical transfer (0.51 $cm^2 \cdot V^{-1} \cdot s^{-1}$). The high mobility can be attributed to the clean interface between WS_2 and MoS_2, which reduces the unwanted defects between layers to improve the charge transfer. Meanwhile, the lateral MoS_2/WS_2 heterojunctions have been demonstrated to be intrinsic monolayer PN junctions without external electrostatic gating.

Afterwards scalable production of few-layer MoS_2/WS_2 vertical heterojunction array was reported by Xue *et al.*[91]

The few-layer MoS_2/WS_2 vertical heterojunctions (Fig. 7(a)) were fabricated by sulfurization of patterned WO_3 and Mo sheets with an ambient pressure thermal reduction process. There are two Raman-active modes ($^1E_{2g}$, A_{1g}) that can be generally observed due to the selection rules for scattering radiation or limited rejection of the Rayleigh scattering radiation.[93] In the Raman spectra of MoS_2/WS_2, the position of $^1E_{2g}$ and A_{1g} peaks do not change, implying that MoS_2 and WS_2 are individual sheets. So the two-step chemical vapor deposition approach has been demonstrated to effectively prevent the mixture of MoS_2 and WS_2, resulting in a well-defined interface between MoS_2 and WS_2. Moreover, the thicknesses of MoS_2 and WS_2 in the heterojunctions can be adjusted by controlling the thicknesses of the predeposited WO_3 and Mo sheets during the fabrication.

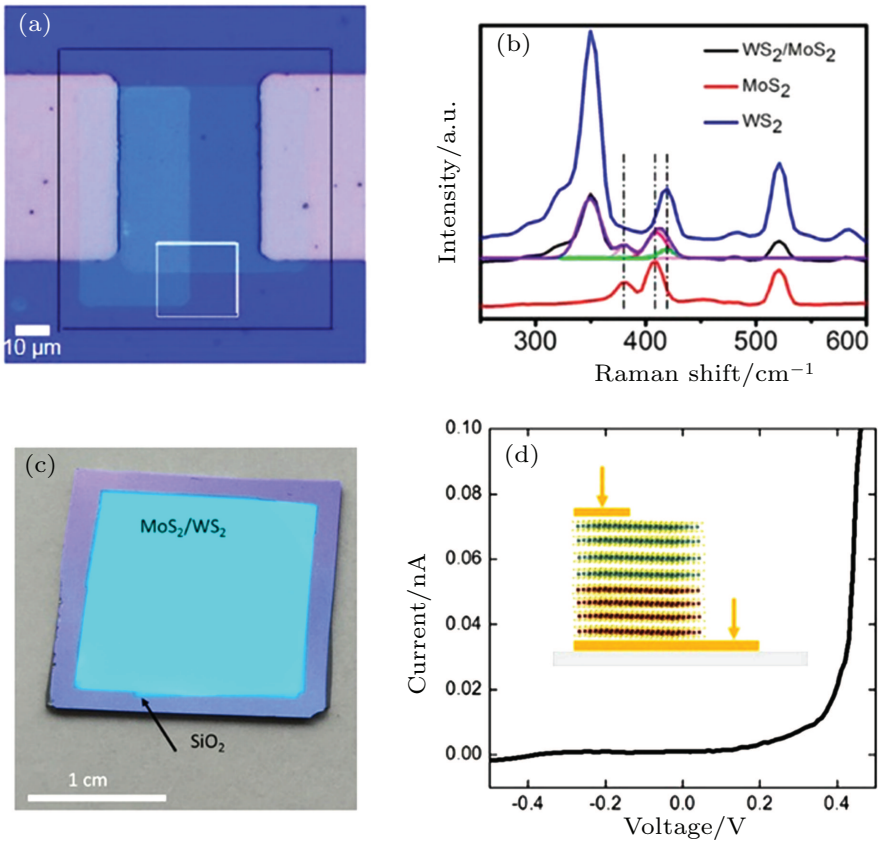


Fig. 7. (color online) (a) Optical micrograph of the MoS_2/WS_2 vertical heterojunction device.[91] (b) Raman spectra of MoS_2, WS_2 and MoS_2/WS_2.[91] (c) Optical image of vertical MoS_2/WS_2heterojunctions grown by chemical vapor deposition.[92] (d) *I*–*V* measurement across a MoS_2/WS_2 heterointerface.[92]

In the same year, Li *et al.* realized the controlled epitaxial growth of lateral WSe_2/MoS_2 heterojunction.[94] WSe_2 was grown on *c*-plane sapphire substrates through van der Waals epitaxy and then MoS_2 was epitaxially grown at the edge of WSe_2. The atomically sharp transition in compositions at junctions can be achieved through precisely controlling the two-step epitaxial growth. Very recently, Choudhary *et al.*[92] reported large-area (> 2 cm^2) vertical MoS_2/WS_2 heterojunctions grown by chemical vapor deposition. The heterojunctions show diode-like current rectification, which means them to be high-quality van der Waals PN junctions (Fig. 7(d)).

To conclude, although mechanical exfoliation and transfer are still widely used to stack two kinds of 2D materials, CVD techniques have been demonstrated to be a reliable way to fabricate large scale vertical and lateral heterojunctions of TMDCs which are more promising for application. Meanwhile, some new methods also appear. Tan *et al.* achieved 2D semiconductor hetero-nanostructures by the epitaxial growth in liquid phase at room temperature.[95] Mahjouri–Samani *et al.* fabricated array of lateral $MoSe_2/MoS_2$ heterojunction by lithographic patterning and controllable conversion of exposed $MoSe_2$ to MoS_2, which also provides some new ideas for device fabrication.[96]

4.2.2. Photoelectric properties of vertical heterojunctions based on only TMDCs

Furchi *et al.*[77] fabricated vertical stacks of WSe_2/MoS_2 exactly by mechanical exfoliation and transfer. The EQE is a low value of about 1.5%. A much higher performance in similar vertical WSe_2/MoS_2 heterojunctions was reported by Cheng *et al.* (Fig. 8(a)).[86]

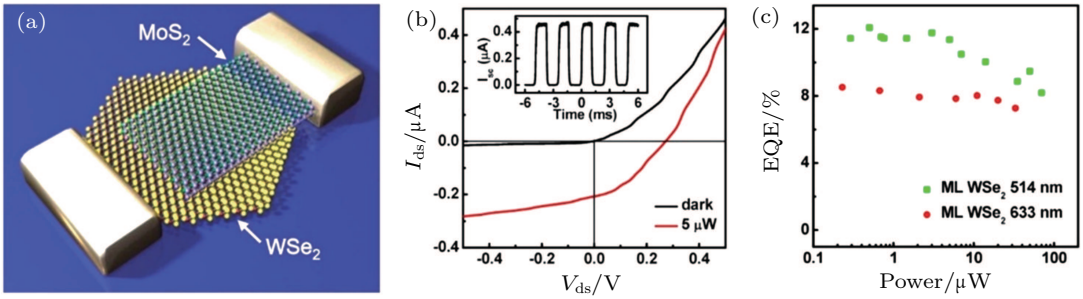


Fig. 8. (color online) (a) Schematic of vertical WSe_2/MoS_2 heterojunction; (b) I_{ds}–V_{ds} curves measured in the dark and under the illumination whose wavelength is 514 nm and power is 5 μW. The inset shows response of the current with respect to periodic on/off of the illumination; (c) EQE under different power of 514 nm and 633 nm laser at $V_{ds} = 0$ and $V_g = 0$.[86]

The vertical WSe_2/MoS_2 heterojunctions have obvious open-circuit voltage and short-circuit current under laser illumination (514 nm, 5 μW) (Fig. 8(b)). Also a fast response time of 100 μs has been demonstrated. The maximum value of EQE can reach 12% under laser illumination (514 nm, 0.5 μW) (Fig. 8(c)) which is higher than homojunctions based on WSe_2.[41,43] The high performance can be resulted from the efficient separation of photocarriers at the interface of WSe_2 and MoS_2.

More recently, in the MoS_2/WSe_2 heterojunction, the ultrafast electron transfer from WSe_2 to MoS_2 sheet was demonstrated to be 470 fs and a 99% efficiency upon optical excitation. This implies MoS_2/WSe_2 heterojunction could have big potential for high-speed photodetectors.[82]

4.2.3. Photoelectric properties of lateral heterojunctions based on only TMDCs

In addition to vertical heterojunctions, lateral 2D heterojunctions have also emerged. Lateral heterojunctions based on TMDCs are commonly fabricated such as $MoSe_2/MoS_2$,[96,97] $MoSe_2/WSe_2$,[98] WS_2/MoS_2,[90] WS_2/WSe_2,[97] WSe_2/MoS_2.[94]

Duan *et al.* realized the lateral epitaxial growth of WS_2/WSe_2 heterojunctions (Fig. 9(a)).[97] Afterwards, a 50-nm-thick Al_2O_3 was deposited on part of WSe_2 to insulate it from the contact for WS_2. Compared with the I_{ds}–V_{ds} curve in the dark, the heterojunctions exhibited obvious photovoltaic with an open-circuit voltage of 0.47 V and short-circuit current of 1.2 nA (Fig. 9(b)). Moreover, the response time is less than 100 μs which is two orders of magnitudes less than the response time of the lateral WSe_2 homojunction.[40] The faster response speed is originated from the carriers transport mainly in surface of lateral heterojunctions. The value of EQE is about 9.9% for these devices. Li *et al.* investigated the WSe_2/MoS_2 lateral heterojunctions.[94] They found that the depletion width of the heterojunction is 320 nm and device shows clear photovoltaic effect.[94]

Moreover, due to the thickness dependence of bandgap and band edges of TMDCs, a novel heterojunctions have appeared, which consist of different layers of the same TMDCs. Interlayer states can exist in these heterojunctions such as monolayer-bilayer WSe_2 heterojunctions[99] and monolayer-multilayer MoS_2 heterojunction.[100,126] Zhang *et al.* studied interlayer states between monolayer and bilayer WSe_2 by low-temperature scanning tunneling microcopy and spectroscopy (STM/S). The interlayer states have a gap value of 0.8 eV as shown in spectrum #13 and spectrum #14 of Fig. 9(e). Because of the interlayer states, the band bending and build-in

electric field can be induced between interfaces (Fig. 9(d)), which implies that they are a novel class of heterojunctions for photodetectors. The advantage of this kind of heterojunctions is that gaps can be adjusted by thickness. Thus through the combination of the same TMDCs of different thickness, detecting wavelength can be tuned and extended.

To conclude, along with development of different techniques, large scale vertical and lateral heterojunctions have been demonstrated and they have exhibited some excellent properties such as the fast response time which is less than 100 μs. Heterojunctions which consist of different layers of the same TMDCs are also greatly promising for new design of photodetectors. Different structures provide a more solid foundation for more complex structures such as PIN junctions and quantum well structures. However, it is still not good enough for applications. For example, the area of heterojunctions with higher quality is not larger enough and EQE is still very low. Hence, the fabrication and performances of TMDC/TMDC heterojunctions all need to be improved.

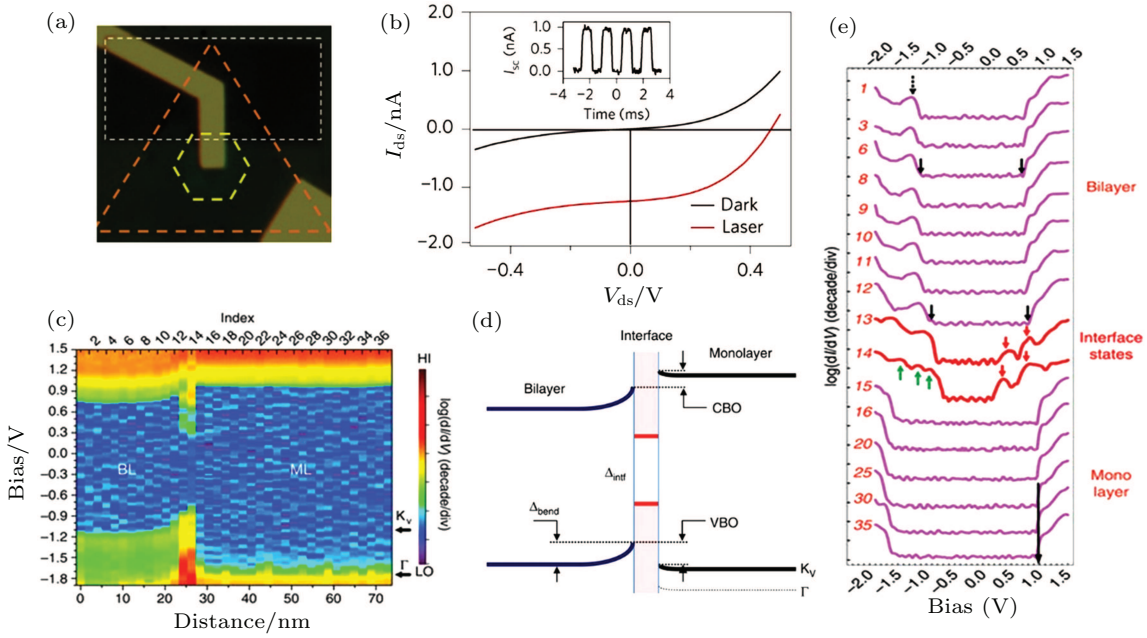


Fig. 9. (color online) (a) Optical image of lateral WS_2/WSe_2 heterojunction.[97] (b) I_{ds}–V_{ds} characteristics in the dark and under laser illumination (514 nm, 30 nW). The inset shows the photocurrent response under periodic on/off laser illumination.[97] (c) Color-coded rendering of the real space imaging of band profile plotted in terms of $\log(\mathrm{d}I/\mathrm{d}V)$ in monolayer-bilayer WSe_2.[99] (d) Band alignment in monolayer-bilayer WSe_2 heterojunctions.[99] (e) Selective subset of $\log(\mathrm{d}I/\mathrm{d}V)$ spectra. The green and red arrows represent valance and conduction band of the interface states.[99]

4.3. Photodetectors based on heterojunctions of TMDCs and other 2D materials

Though TMDCs have the advantage of strong light absorption, applications based on TMDCs are limited by the natures such as low carrier mobility compared with graphene[2,5,101] and few-layer black phosphorus.[102–104] Thus, in order to make devices with better performance, a native way is to combine good properties of TMDCs and the advantages of other 2D materials by stacking their layers together.

The approach has already been demonstrated by Deng *et al.*[105] The MoS_2/BP heterojunctions combine high carrier mobility of BP with strong light absorption of MoS_2. The heterojunctions show high responsivity of 418 $mA{\cdot}W^{-1}$, but low EQE of 0.3%. Due to built-in electric field, the photocarriers can be effectively separated and then the photoelectrons are injected into BP layer, rather than trapped in MoS_2.

More recently, the similar study of WSe_2/BP heterojunctions (Fig. 10(a)) were reported by Chen *et al.*[106] Due to the weak screening effect and the ambipolar transport of WSe_2[40–42,55] and BP,[103,107] different types of heterojunctions can be well controlled by electrostatic gating. As shown in Figs. 10(b) and 10(c), the rectification properties almost disappear when $V_g > -33$ V and $V_g < 25$ V. The values of EQE are shown in Fig. 8(d) and the maximum value is 3.1% at $V_g = 31$ V, which is larger than 0.3% in the MoS_2/BP heterojunctions.[105] By stacking TMDCs and other 2D materials together, their merits can be combined in the same device such as the bipolar transport of WSe_2 and BP, light absorption of MoS_2 and high mobility of graphene, and so on.[108–111]

Although the junctions have shown excellent properties, there are still many methods to improve performances by using graphene as electrodes to reduce the influence of barrier,[112,113] facilitating the carrier collection by designing a vertical sandwiched structure[76,113,114] and using BN as a dielectric layer to improve interface and increase the reflection between the layers.[56,115]

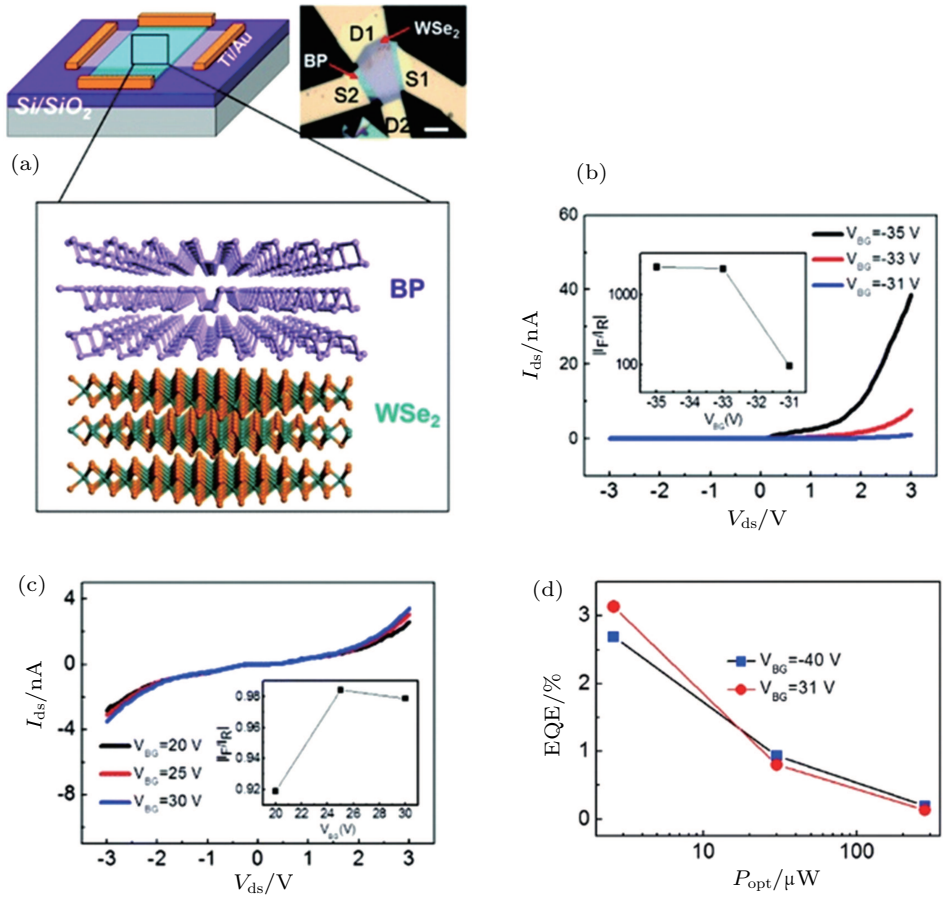


Fig. 10. (color online) (a) Device schematic diagram and optical image of WSe_2/BP heterojunction. (b) and (c) I_{ds}–V_{ds} characteristics under different V_g. The insets show the rectification ratio with respect to V_g. (d) Relations between EQE and power of laser under $V_g = -40$ V and $V_g = 31$ V.[106]

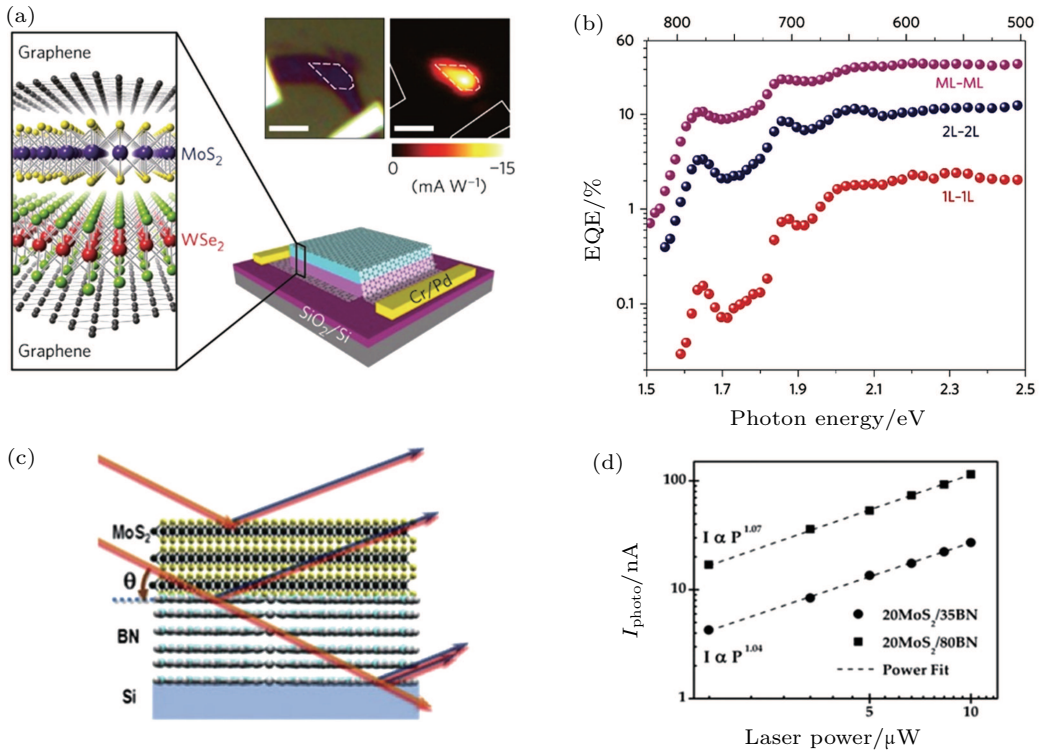


Fig. 11. (color online) (a) Schematic diagram of MoS_2/WSe_2 junction sandwiched between top and bottom graphene electrodes.[76] (b) The relationship between EQE and excitation energy.[76] (c) Possible existence of the interfaces between materials. (d) Photocurrent with respect to laser power.[115]

Early Luo *et al.* has proven the response time of photodetectors based on InSe can be decreased to 120 μs by using graphene as electrodes, which is about 40 times faster than the detectors using metal electrodes.[112] Lee *et al.* fabricated vertical MoS_2/WSe_2 heterojunction by using top and bottom graphene electrodes (Fig. 11(a)).[76] The device had photoresponsivity of ~ 10 mA·W^{-2}, which is five times larger than that of MoS_2/WSe_2 heterojunction with metal contacts. There are several advantages to use graphene as electrodes. Firstly ultrafast carrier mobility of graphene is very useful in the separation of photogenerated carriers, which can enhance the photoresponsivity and further improve detectivity. Secondly the graphene can absorb few light which has little effects on the light absorption of the heterostructure. Finally the overlapping of the top graphene and bottom graphene facilitates the carrier collection by reducing the vertical transport channel, which can also improve the response speed. So using graphene as electrodes to improve the performances of photodetectors based on TMDCs and other 2D materials was demonstrated to be an effective way.

Except using graphene as electrodes, in order to improve the performances of TMDCs, Wasala *et al.* investigated the effects of BN on the optical properties of MoS_2.[115] As shown in Fig. 11(d), the photocurrent increased with increasing the thickness of the underlying BN layer. Because the BN layers can increase the reflections between layers, which can result in the enhancement of photocurrent. It implies BN also can be used to enhance the photocurrent response properties of TMDCs such as photoresponsivity and detectivity. Moreover because the h-BN has atomically flat and smooth surface with lack of dangling bonds, it has been widely used as an ideal subatrate and dielectric layer for 2D materials such as graphene and TMDCs.[56,116,117] The h-BN can also be used as intercalation which could decrease the dark current and further improve detectivity.[61]

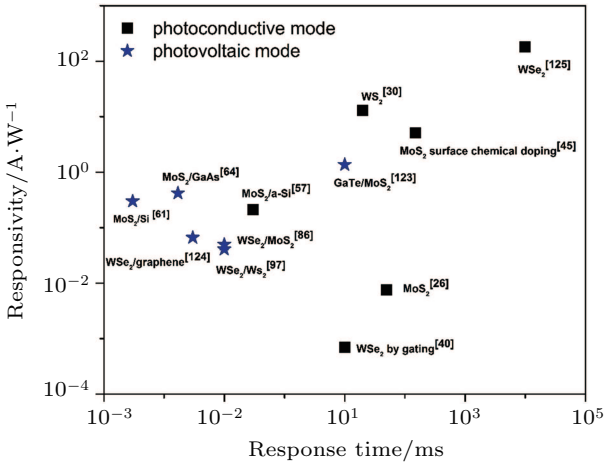


Fig. 12. (color online) Responsivity against response time for some devices reviewed.

Table 1. Summary of literature data for photodetectors based on two-dimensional TMDCs. The table contains the configuration, the fabrication technology, mode, and some benchmark parameters (external quantum efficiency (EQE), responsivity (R), specific detectivity (D^*), rise time (τ_r)).

Material (Configuration)	Technology	Mode	Figures of merit				Ref.
			EQE/%	R/A·W^{-1}	D^*/Jones	τ_r/ms	
Single-layer MoS_2(FET)	Mechanical exfoliation	photoconductive	NA	0.0075	NA	50	[26]
		photoconductive	NA	880	NA	$>10^4$	[31]
Multilayer MoS_2 (FET)	Mechanical exfoliation	photoconductive	NA	~ 0.12	$\sim 10^{11}$	NA	[53]
MoS_2 (Vertical Homojunction)	Plasma doping	photovoltaic	78	NA	NA	NA	[52]
MoS_2 (Lateral homojunction)	Surface chemical doping	photoconductive	1200	5.07	3×10^{10}	100-200	[46]
		photoconductive	81	0.33	1.6×10^{10}	NA	
n-$MoSe_2$/p-$MoSe_2$ (Vertical homojunction)	Elemental doping, mechanical exfoliation and transfer	photoconductive	1049	~ 3	NA	NA	[50]
WSe_2(Lateral homojunction)	Electrostatic gating, mechanical exfoliation and transfer	photoconductive	0.1	7×10^{-4}	NA	~ 10	[40]
		photovoltaic	0.2	NA	NA	NA	[41]
MoS_2/Si (Heterojunction)	Magnetron sputter	photovoltaic	NA	0.3	10^{13}	3×10^{-3}	[61]
	Mechanical exfoliation and transfer	photoconductive	NA	7.2	$\sim 7\times10^{9}$	NA	[60]
MoS_2/GaAs (Heterojunction)	CVD	photovoltaic	NA	0.419	1.9×10^{14}	0.017	[64]
C_8-BTBT/ MoS_2 (Heterojunction)	Mechanical exfoliation and epitaxial growth	photovoltaic	NA	0.022	NA	NA	[70]
WSe_2/ MoS_2 (Vertical heterojunction)	PVD and mechanical exfoliation and transfer	photovoltaic	12	NA	NA	<0.1	[86]
WS_2/WSe_2 (Lateral heterojunction)	CVD	photovoltaic	9.9	NA	NA	<0.1	[97]
MoS_2/BP (Vertical heterojunction)	CVD and mechanical exfoliation and transfer	photovoltaic	0.3	NA	NA	NA	[105]
		photoconductive	NA	0.418	NA	NA	
WSe_2/BP (Vertical heterojunction)	Mechanical exfoliation and transfer	photovoltaic	3.1	NA	NA	NA	[106]

In conclusion, completely vertical structure can reduce the transport channel length, which can greatly enhance the photoresponse speed of photodetectors. Moreover, using graphene electrodes and BN reflection layer have been demonstrated to be promising methods to improve photocurrent response. Combing those methods, high-speed and highly sensitive photodetector could be realized by stacking of TMDCs and other two-dimensional materials.

Figure 12 and Table 1 summarize some experimental results from 2D material photodetectors in the review. The responsivity and response time for part of the reviewed devices are summarized in Fig. 12. In Table 1, we list the configuration, the fabrication technology, EQE, responsivity, specific detectivity and rise time. All those present the performances of the detectors.

5. Conclusion and perspectives

This review provides an overview of the recent development in photodetectors based on junctions of TMDCs from structures, fabrications and performances. Owing to the built-in electric field in those junctions, the photogenerated electrons and holes can be more effectively separated. So compared with photodetectors based on FET type of intrinsic TMDCs, photodetectors based on junctions of TMDCs show many advantages (such as lager responsivity or faster response speed) as shown in Table 1 and Fig. 12. Moreover, selection of the materials and the device fabrication processing all have great influence on the performance of photodetectors.

Homojunctions can be created by the following three methods: surface chemical doping, elemental doping and electrostatic gating. Although surface chemical doping is suitable for thin layers of TMDCs, the homojunctions based on the surface chemical doping are easy to be affected by the external environment. Elemental doping is a fesiable way for vertical stable homojunctions with high performance. Although electrostatic gating can also be used to create homojunctions, the EQE of these junctions is still very low. Because of the limination of charge mobility, lateral homojunctions fabricated by surface chemical doping and electrostaic show slow photoresponse. However, homojunctions are based on the similiar materials, which makes them easier to realize the sensitive detection of special wavelength.

Heterojunctions can be fabricated by mechanical exfoliation and transfer, CVD and some other methods. Compared with mechanical exfoliation and transfer, CVD method has been demonstrated to be the most effective and promising method to obtain large scale heterojunctions based on TMDCs with atomically sharp interface. Moreover, CVD-grown junctions showed stronger interlayer interaction compared with transferred counterparts.

In vertical heterojunctions, using graphene as top and bottom electrodes can effectively shorten the vertical transport distance of photogenerated carriers, which reduces the response time by several orders of magnitude. The photoresponse can be stongly enhanced using BN as the reflection layer. Taking the advantages of graphene and BN, the heterojunciton photodetectors should have potential appliacations in high speed and weak signal photodetections.

Photodetectors with wide response spectrum are important in many applications. Heterojunctions can combine TMDCs and other semiconductor materials with different absorption wavelength together. MoS_2/GaAs heterojunctions have been already demonstrated to have wide spectrum response from ultraviolet to visible light. Thus by selecting two appropriate materials in heterojunctions, it has great potential to realize from ultraviolet to far infrared wider response spectrum photodetectors or multicolor photodetectors.

Moreover, in TMDCs, spin and valley degrees of freedom are intimately coupled due to inversion symmetry breaking together with strong spin–orbit interaction, which has also attracted a great deal of interest.[118] By circularly polarized optical pumping, spin-valley coupled polarization can be generated,[119] which has been observed in optoeletronic devices based on MoS_2[120] and WSe_2.[121,122] It should be of great significance to introduce spin-polarization and valley-polarization in photodetectors based on junctions of TMDCs.

With the development of TMDCs, different types of junctions based on these materials have been demonstrated in photodetections. However, there is still a long way before they can be actually applied. In application, more controllable and effective way to fabricate large scale junctions is highly desired. Also the stability of these junctions still needs to be improved. Moreover, in theory, electronic transport in heterojunctions has been studied for many years by conventional modes, which cannot be applied well in few layer cases. A comprehensive understanding of electronic transport in heterojunctions based on 2D materials is urgently needed. Nevertheless, these junctions will greatly enrich studies in photodetectors based on the junctions of TMDCs.

References

[1] Novoselov K S, Geim A K, Morozov S, Jiang D, Zhang Y, Dubonos S A, Grigorieva I and Firsov A 2004 *Science* **306** 666
[2] Novoselov K, Geim A K, Morozov S, Jiang D, Katsnelson M, Grigorieva I, Dubonos S and Firsov A 2005 *Nature* **438** 197
[3] Novoselov K, Jiang D, Schedin F, Booth T, Khotkevich V, Morozov S and Geim A 2005 *Proc. Natl. Acad. Sci. USA* **102** 10451
[4] Lee C, Wei X, Kysar J W and Hone J 2008 *Science* **321** 385
[5] Xia F, Mueller T, Lin Y M, Valdes-Garcia A and Avouris P 2009 *Nat. Nanotech.* **4** 839
[6] Mueller T, Xia F and Avouris P 2010 *Nat. Photon.* **4** 297
[7] Wang L, Meric I, Huang P, Gao Q, Gao Y, Tran H, Taniguchi T, Watanabe K, Campos L and Muller D 2013 *Science* **342** 614
[8] Butler S Z, Hollen S M, Cao L, Cui Y, Gupta J A, Gutiérrez H R, Heinz T F, Hong S S, Huang J and Ismach A F 2013 *ACS Nano* **7** 2898
[9] Xu M, Liang T, Shi M and Chen H 2013 *Chem. Rev.* **113** 3766
[10] Koski K J and Cui Y 2013 *ACS Nano* **7** 3739
[11] Das S, Robinson J A, Dubey M, Terrones H and Terrones M 2015 *Annu. Rev. Mater. Res.* **45** 1
[12] Mak K F, Lee C, Hone J, Shan J and Heinz T F 2010 *Phys. Rev. Lett.* **105** 136805

[13] Radisavljevic B, Radenovic A, Brivio J, Giacometti V and Kis A 2011 *Nat. Nanotech.* **6** 147
[14] Wang Q H, Kalantar-Zadeh K, Kis A, Coleman J N and Strano M S 2012 *Nat. Nanotech.* **7** 699
[15] Chhowalla M, Shin H S, Eda G, Li L J, Loh K P and Zhang H 2013 *Nat. Chem.* **5** 263
[16] Wilson J and Yoffe A 1969 *Adv. Phys.* **18** 193
[17] Frindt R F and Yoffe A D 1963 *Pro. R. Soc. London A: Mathematical, Physical and Engineering Sciences* **273** 69
[18] Cao Y F, Cai K M, Li L J, Lu W J, Sun Y P and Wang K Y 2014 *Chin. Phys. Lett.* **31** 077203
[19] Costanzo D, Jo S, Berger H and Morpurgo A F 2016 *Nat. Nanotech.* **11** 339
[20] Ayari A, Cobas E, Ogundadegbe O and Fuhrer M S 2007 *J. Appl. Phys.* **101** 14507
[21] Splendiani A, Sun L, Zhang Y, Li T, Kim J, Chim C Y, Galli G and Wang F 2010 *Nano Lett.* **10** 1271
[22] Eda G, Yamaguchi H, Voiry D, Fujita T, Chen M and Chhowalla M 2011 *Nano Lett.* **11** 5111
[23] Yun W S, Han S, Hong S C, Kim I G and Lee J 2012 *Phys. Rev. B* **85** 033305
[24] Liu Z, Lau S P and Yan F 2015 *Chem. Soc. Rev.* **44** 5638
[25] Geim A K and Grigorieva I V 2013 *Nature* **499** 419
[26] Yin Z, Li H, Li H, Jiang L, Shi Y, Sun Y, Lu G, Zhang Q, Chen X and Zhang H 2012 *ACS Nano* **6** 74
[27] Larentis S, Fallahazad B and Tutuc E 2012 *Appl. Phys. Lett.* **101** 223104
[28] Wu C C, Jariwala D, Sangwan V K, Marks T J, Hersam M C and Lauhon L J 2013 *J. Phys. Chem. Lett.* **4** 2508
[29] Das S and Appenzeller J 2013 *Appl. Phys. Lett.* **103** 103501
[30] Huo N, Yang S, Wei Z, Li S S, Xia J B and Li J 2014 *Sci. Rep.* **4** 5209
[31] Lopez-Sanchez O, Lembke D, Kayci M, Radenovic A and Kis A 2013 *Nat. Nanotech.* **8** 497
[32] Wang H, Liu F, Fu W, Fang Z, Zhou W and Liu Z 2014 *Nanoscale* **6** 12250
[33] Koppens F H, Mueller T, Avouris P, Ferrari A C, Vitiello M S and Polini M 2014 *Nat. Nanotech.* **9** 780
[34] Zhang W, Wang Q, Chen Y, Wang Z and Wee A T 2016 *2D Mater.* **3** 022001
[35] Bablich A, Kataria S and Lemme M 2016 *Electronics* **5** 13
[36] Pospischil A and Mueller T 2016 *Appl. Sci.* **6** 78
[37] Farmer D B, Golizadeh-Mojarad R, Perebeinos V, Lin Y-M, Tulevski G S, Tsang J C and Avouris P 2009 *Nano Lett.* **9** 388
[38] Peters E C, Lee E J, Burghard M and Kern K 2010 *Appl. Phys. Lett.* **97** 193102
[39] Lemme M C, Koppens F H, Falk A L, Rudner M S, Park H, Levitov L S and Marcus C M 2011 *Nano Lett.* **11** 4134
[40] Groenendijk D J, Buscema M, Steele G A, Michaelis de Vasconcellos S, Bratschitsch R, van der Zant H S and Castellanos-Gomez A 2014 *Nano Lett.* **14** 5846
[41] Baugher B W, Churchill H O, Yang Y and Jarillo-Herrero P 2014 *Nat. Nanotech.* **9** 262
[42] Ross J S, Klement P, Jones A M, Ghimire N J, Yan J, Mandrus D, Taniguchi T, Watanabe K, Kitamura K and Yao W 2014 *Nat. Nanotech.* **9** 268
[43] Pospischil A, Furchi M M and Mueller T 2014 *Nat. Nanotech.* **9** 257
[44] Buscema M, Groenendijk D J, Steele G A, van der Zant H S and Castellanos-Gomez A 2014 *Nat. Commun.* **5** 4651
[45] Fang H, Tosun M, Seol G, Chang T C, Takei K, Guo J and Javey A 2013 *Nano Lett.* **13** 1991
[46] Choi M S, Qu D, Lee D, Liu X, Watanabe K, Taniguchi T and Yoo W J 2014 *ACS Nano* **8** 9332
[47] Yang L, Majumdar K, Liu H, Du Y, Wu H, Hatzistergos M, Hung P, Tieckelmann R, Tsai W and Hobbs C 2014 *Nano Lett.* **14** 6275
[48] Lei S, Wang X, Li B, Kang J, He Y, George A, Ge L, Gong Y, Dong P and Jin Z 2016 *Nat. Nanotech.* **11** 465
[49] Suh J, Park T E, Lin D Y, Fu D, Park J, Jung H J, Chen Y, Ko C, Jang C and Sun Y 2014 *Nano Lett.* **14** 6976
[50] Jin Y, Keum D H, An S J, Kim J, Lee H S and Lee Y H 2015 *Adv. Mater.* **27** 5534
[51] Fang H, Chuang S, Chang T C, Takei K, Takahashi T and Javey A 2012 *Nano Lett.* **12** 3788
[52] Wi S, Kim H, Chen M, Nam H, Guo L J, Meyhofer E and Liang X 2014 *ACS Nano* **8** 5270
[53] Choi W, Cho M Y, Konar A, Lee J H, Cha G B, Hong S C, Kim S, Kim J, Jena D and Joo J 2012 *Adv. Mater.* **24** 5832
[54] Kim E, Ko C, Kim K, Chen Y, Suh J, Ryu S G, Wu K, Meng X, Suslu A and Tongay S 2016 *Adv. Mater.* **28** 341
[55] Huo N, Yang J, Huang L, Wei Z, Li S S, Wei S H and Li J 2015 *Small* **11** 5430
[56] Flöry N, Jain A, Bharadwaj P, Parzefall M, Taniguchi T, Watanabe K and Novotny L 2015 *Appl. Phys. Lett.* **107** 123106
[57] Esmaeili-Rad M R and Salahuddin S 2013 *Sci. Rep.* **3** 2345
[58] Lopez-Sanchez O, Dumcenco D, Charbon E and Kis A 2014 arXiv:1411.3232 [cond-mat.mes-hall]
[59] Lopez-Sanchez O, Alarcon Llado E, Koman V, Fontcuberta i Morral A, Radenovic A and Kis A 2014 *ACS Nano* **8** 3042)
[60] Li Y, Xu C Y, Wang J Y and Zhen L 2014 *Sci. Rep.* **4** 7186
[61] Wang L, Jie J, Shao Z, Zhang Q, Zhang X, Wang Y, Sun Z and Lee S T 2015 *Adv. Funct. Mater.* **25** 2910
[62] Hao L, Liu Y, Gao W, Han Z, Xue Q, Zeng H, Wu Z, Zhu J and Zhang W 2015 *J. Appl. Phys.* **117** 114502
[63] Chuang S, Kapadia R, Fang H, Chang T C, Yen W C, Chueh Y L and Javey A 2013 *Appl. Phys. Lett.* **102** 242101
[64] Xu Z, Lin S, Li X, Zhang S, Wu Z, Xu W, Lu Y and Xu S 2016 *Nano Energy* **23** 89
[65] Ruzmetov D, Zhang K, Stan G, Kalanyan B, Bhimanapati G R, Eichfeld S M, Burke R A, Shah P B, O'Regan T P and Crowne F J 2016 *ACS Nano* **10** 3580
[66] Tsai D S, Liu K K, Lien D H, Tsai M L, Kang C F, Lin C A, Li L J and He J H 2013 *Acs Nano* **7** 3905
[67] Jariwala D, Howell S L, Chen K S, Kang J, Sangwan V K, Filippone S A, Turrisi R, Marks T J, Lauhon L J and Hersam M C 2016 *Nano Lett.* **16** 497
[68] Kim K, Santos E J, Lee T H, Nishi Y and Bao Z 2015 *Small* **11** 2037
[69] Wu B, Zhao Y, Nan H, Yang Z, Zhang Y, Zhao H, He D, Jiang Z, Liu X and Li Y 2016 *Nano Lett.* **16** 3754
[70] He D, Pan Y, Nan H, Gu S, Yang Z, Wu B, Luo X, Xu B, Zhang Y and Li Y 2015 *Appl. Phys. Lett.* **107** 183103
[71] He D, Zhang Y, Wu Q, Xu R, Nan H, Liu J, Yao J, Wang Z, Yuan S and Li Y 2014 *Nat. Commun.* **5** 5162
[72] Zhang L, Yang Y, Huang H, Lyu L, Zhang H, Cao N, Xie H, Gao X, Niu D and Gao Y 2015 *J. Phys. Chem. C* **119** 4217
[73] Zheng Y J, Huang Y L, Chen Y, Zhao W, Eda G, Spataru C D, Zhang W, Chang Y H, Li L J and Chi D 2016 *ACS Nano* **10** 2476
[74] Hong X, Kim J, Shi S F, Zhang Y, Jin C, Sun Y, Tongay S, Wu J, Zhang Y and Wang F 2014 *Nat. Nanotech.* **9** 682
[75] Tongay S, Fan W, Kang J, Park J, Koldemir U, Suh J, Narang D S, Liu K, Ji J and Li J 2014 *Nano Lett.* **14** 3185
[76] Lee C H, Lee G H, Van Der Zande A M, Chen W, Li Y, Han M, Cui X, Arefe G, Nuckolls C and Heinz T F 2014 *Nat. Nanotech.* **9** 676
[77] Furchi M M, Pospischil A, Libisch F, Burgdoörfer J and Mueller T 2014 *Nano Lett.* **14** 4785
[78] Chiu M H, Li M Y, Zhang W, Hsu W T, Chang W H, Terrones M, Terrones H and Li L J 2014 *ACS Nano* **8** 9649
[79] Fang H, Battaglia C, Carraro C, Nemsak S, Ozdol B, Kang J S, Bechtel H A, Desai S B, Kronast F and Unal A A 2014 *Proc. Natl. Acad. Sci.* **111** 6198
[80] Chiu M H, Zhang C, Shiu H W, Chuu C P, Chen C H, Chang C Y S, Chen C H, Chou M Y, Shih C K and Li L J 2015 *Nat. Commun.* **6** 7666
[81] Nourbakhsh A, Zubair A, Dresselhaus M S and Palacios T 2016 *Nano Lett.* **16** 1359
[82] Peng B, Yu G, Liu X, Liu B, Liang X, Bi L, Deng L, Sum T C and Loh K P 2016 *2D Mater.* **3** 025020
[83] Ceballos F, Bellus M Z, Chiu H Y and Zhao H 2014 *ACS Nano* **8** 12717
[84] Zhang K, Zhang T, Cheng G, Li T, Wang S, Wei W, Zhou X, Yu W, Sun Y and Wang P 2016 *ACS Nano* **10** 3852
[85] Rivera P, Schaibley J R, Jones A M, Ross J S, Wu S, Aivazian G, Klement P, Seyler K, Clark G and Ghimire N J 2015 *Nat. Commun.* **6** 6242
[86] Cheng R, Li D, Zhou H, Wang C, Yin A, Jiang S, Liu Y, Chen Y, Huang Y and Duan X 2014 *Nano Lett.* **14** 5590
[87] Lee Y H, Zhang X Q, Zhang W, Chang M T, Lin C T, Chang K D, Yu Y C, Wang J T W, Chang C S and Li L J 2012 *Adv. Mater.* **24** 2320
[88] Liu K K, Zhang W, Lee Y H, Lin Y C, Chang M T, Su C Y, Chang C S, Li H, Shi Y and Zhang H 2012 *Nano Lett.* **12** 1538

[89] van der Zande A M, Huang P Y, Chenet D A, Berkelbach T C, You Y, Lee G H, Heinz T F, Reichman D R, Muller D A and Hone J C 2013 *Nat. Mater.* **12** 554

[90] Gong Y, Lin J, Wang X, Shi G, Lei S, Lin Z, Zou X, Ye G, Vajtai R and Yakobson B I 2014 *Nat. Mater.* **13** 1135

[91] Xue Y, Zhang Y, Liu Y, Liu H, Song J, Sophia J, Liu J, Xu Z Q, Xu Q and Wang Z 2016 *ACS Nano* **10** 573

[92] Choudhary N, Park J, Hwang J Y, Chung H S, Dumas K H, Khondaker S I, Choi W and Jung Y 2016 *Sci. Rep.* **6** 25456

[93] Verble J, Wietling T and Reed P 1972 *Solid State Commun.* **11** 941

[94] Li M Y, Shi Y, Cheng C C, Lu L S, Lin Y C, Tang H L, Tsai M L, Chu C W, Wei K H and He J H 2015 *Science* **349** 524

[95] Tan C, Zeng Z, Huang X, Rui X, Wu X J, Li B, Luo Z, Chen J, Chen B and Yan Q 2015 *Angew. Chem.* **127** 1861

[96] Mahjouri-Samani M, Lin M W, Wang K, Lupini A R, Lee J, Basile L, Boulesbaa A, Rouleau C M, Puretzky A A and Ivanov I N 2015 *Nat. Commun.* **6** 7749

[97] Duan X, Wang C, Shaw J C, Cheng R, Chen Y, Li H, Wu X, Tang Y, Zhang Q and Pan A 2014 *Nat. Nanotech.* **9** 1024

[98] Huang C, Wu S, Sanchez A M, Peters J J, Beanland R, Ross J S, Rivera P, Yao W, Cobden D H and Xu X 2014 *Nat. Mater.* **13** 1096

[99] Zhang C, Chen Y, Huang J K, Wu X, Li L J, Yao W, Tersoff J and Shih C K 2016 *Nat. Commun.* **7** 10349

[100] Howell S L, Jariwala D, Wu C C, Chen K S, Sangwan V K, Kang J, Marks T J, Hersam M C and Lauhon L J 2015 *Nano Lett.* **15** 2278

[101] Avouris P, Chen Z and Perebeinos V 2007 *Nat. Nanotech.* **2** 605

[102] Koenig S P, Doganov R A, Schmidt H, Neto A C and Oezyilmaz B 2014 *Appl. Phys. Lett.* **104** 103106

[103] Li L, Yu Y, Ye G J, Ge Q, Ou X, Wu H, Feng D, Chen X H and Zhang Y 2014 *Nat. Nanotech.* **9** 372

[104] Liu H, Neal A T, Zhu Z, Luo Z, Xu X, Tománek D and Ye P D 2014 *ACS Nano* **8** 4033

[105] Deng Y, Luo Z, Conrad N J, Liu H, Gong Y, Najmaei S, Ajayan P M, Lou J, Xu X and Ye P D 2014 *ACS Nano* **8** 8292

[106] Chen P, Zhang T, Zhang J, Xiang J, Yu H, Wu S, Lu X, Wang G, Wen F and Liu Z 2016 *Nanoscale* **8** 3254

[107] Xia F, Wang H and Jia Y 2014 *Nat. Commun.* **5** 4458

[108] Zhang W, Chuu C P, Huang J K, Chen C H, Tsai M L, Chang Y H, Liang C T, Chen Y Z, Chueh Y L and He J H 2014 *Sci. Rep.* **4** 3826

[109] Henck H, Pierucci D, Chaste J, Naylor C H, Avila J, Balan A, Silly M G, Asensio M C, Sirotti F and Johnson A C 2016 *Appl. Phys. Lett.* **109** 113103

[110] Li B, Huang L, Zhong M, Li Y, Wang Y, Li J and Wei Z 2016 *Adv. Electron. Mater.* **2** 1600298

[111] Yang J, Huo N, Li Y, Jiang X W, Li T, Li R, Lu F, Fan C, Li B and Nørgaard K 2015 *Adv. Electron. Mater.* **1** 1500267

[112] Luo W, Cao Y, Hu P, Cai K, Feng Q, Yan F, Yan T, Zhang X and Wang K 2015 *Adv. Opt. Mater.* **3** 1418

[113] Yan F, Zhang D, Luo W, Hu P, Feng Q, Shen C, Wei X, Chang K and Wang K 2016 rXiv:1606.05469

[114] Yu W J, Liu Y, Zhou H, Yin A, Li Z, Huang Y and Duan X 2013 *Nat. Nanotech.* **8** 952

[115] Wasala M, Zhang J, Ghosh S, Muchharla B, Malecek R, Mazumdar D, Samassekou H, Gaither-Ganim M, Morrison A and Lopez N P 2016 *J. Mater. Res.* **31** 893

[116] Lee G H, Yu Y J, Cui X, Petrone N, Lee C H, Choi M S, Lee D Y, Lee C, Yoo W J and Watanabe K 2013 *ACS Nano* **7** 7931

[117] Cui X, Lee G H, Kim Y D, Arefe G, Huang P Y, Lee C H, Chenet D A, Zhang X, Wang L and Ye F 2015 *Nat. Nanotech.* **10** 534

[118] Xiao D, Liu G B, Feng W, Xu X and Yao W 2012 *Phys. Rev. Lett.* **108** 196802

[119] Xu X, Yao W, Xiao D and Heinz T F 2014 *Nat. Phys.* **10** 343

[120] Eginligil M, Cao B, Wang Z, Shen X, Cong C, Shang J, Soci C and Yu T 2015 *Nat. Commun.* **6** 7636

[121] Yuan H, Wang X, Lian B, Zhang H, Fang X, Shen B, Xu G, Xu Y, Zhang S C and Hwang H Y 2014 *Nat. Nanotech.* **9** 851

[122] Zhang Y, Oka T, Suzuki R, Ye J and Iwasa Y 2014 *Science* **344** 725

[123] Yang S, Wang C, Ataca C, Li Y, Chen H, Cai H, Suslu A, Grossman J C, Jiang C and Liu Q 2016 *ACS Appl. Mater. Inter.* **8** 2533

[124] Gao A, Liu E, Long M, Zhou W, Wang Y, Xia T, Hu W, Wang B and Miao F 2016 *Appl. Phys. Lett.* **108** 223501

[125] Zhang W, Chiu M H, Chen C H, Chen W, Li L J and Wee A T S 2014 *ACS Nano* **8** 8653

[126] Kallatt S, Umesh G, Bhat N and Majumdar K 2016 *Nanoscale* **8** 15213